Experimental Charge Densities and Intermolecular Interactions: Electrostatic and Topological Analysis of DL-Histidine

Philip Coppens,*,† Yuriy Abramov,† Michael Carducci,†,1 Boris Korjov,† Irina Novozhilova,† Cristobal Alhambra,† and Mark R. Pressprich‡

Contribution from the Department of Chemistry, State University of New York at Buffalo, Buffalo, New York 14260-3000, and Bruker Analytical X-ray Systems, Inc., 6300 Enterprise Lane, Madison, Wisconsin 53719-1173

Received September 17, 1998

Abstract: A high-resolution, low-temperature X-ray diffraction data set on DL-histidine, collected with a CCD detector, is used in the analysis of molecular bonding and intermolecular interactions. The molecular dipole moment in the crystal is enhanced relative to that from HF and DFT calculations. Topological properties of the molecular electron density differ from theory for the polar bonds but generally agree well for the C−C bonds in the molecule. A major aim of the study is the evaluation of the electrostatic contribution to the intermolecular interactions from the experimental density. The electrostatic interaction energies between pairs of neighboring molecules, as calculated from the experimental density, compare reasonably well with the total interaction energies from supermolecule calculations. The agreement is somewhat improved by the addition of nonelectrostatic repulsion and dispersive terms, which together contribute much less than the electrostatic energy. The electrostatic interaction energy calculated from the CHARMM point-charge force field is often close to the values derived from the experimental charge density, though exceptions occur. In an alternative approach, the topology of the intermolecular charge density is related to the intermolecular interaction energy. The latter approach makes use of a density functional by Abramov (*Acta Crystallogr*. **1997**, *A53*, 264−272) and a relation between the potential energy density at the bond critical point and the hydrogen bond dissociation energy (Espinosa, et al. *Chem. Phys. Lett*. **1998**, *285*, 170−173).

Introduction

As a result of recent experimental and computational developments, experimental charge densities can now be used to analyze a range of problems of chemical interest.[2] Area detectors have greatly speeded up data collection and led to a significant increase of redundancy in the data sets. An extensively tested software package that incorporates the aspherical atom multipole refinement procedure and calculates electrostatic quantities from the results has simplified the subsequent analysis. As a result, a typical charge density study can now be performed in a few days or less, provided a good quality crystal is available.

An application of considerable interest concerns the calculation of the Coulombic molecular interactions directly from the experimental density.[3] For crystals containing polar molecules, electrostatic interactions give a major contribution to the total interaction energy. In most current work, their calculation is based on a theoretical charge distribution for isolated molecules, usually excluding electron correlation. By comparison, the experimental results provide the actual charge density in the crystal, which includes the effects of the molecular interactions. The calculation can be based on the atom-centered multipoles, which follow from the aspherical atom refinements. The atom-centered multipole description used in the experimental treatment of the X-ray data is related to the *distributed multipole model* used by Stone at al. in the calculation of intermolecular forces. If the sites of the distributed multipole model are limited to the atomic positions, the two models are identical.

A second approach relating the charge density to the energy of intermolecular interaction is based on topological analysis. Theoretical studies on a number of bimolecular complexes have shown that the hydrogen bond dissociation energy is related to the topology of the charge density at the bond critical point in the bond path linking the H-atom with the acceptor atom. Boyd and Choi were the first to derive a linear relation between the density at the critical point ρ_{CP} and the hydrogen bond dissociation energy.[4] More extensive studies relating the topology and the properties of hydrogen bonds were reported by Carroll, Chang, and Bader[5] and Koch and Popelier.[6] From analysis of experimental densities for a set of 83 X−H···O (X = C, N, O) interactions, Espinosa, Molins, and Lecomte[7] derived a relation between the potential energy density at the bond critical point, V_{CP}, and the hydrogen bond dissociation energy. The required values of V_{CP} are obtained from the experimental densities through a functional derived by Abramov.[8]

† SUNY at Buffalo.

‡ Bruker Analytical X-ray Systems.

(1) Current address: Department of Chemistry, University of Arizona, Tucson, AZ 85721-0041.

(2) Coppens, P. *X-ray Charge Densities and Chemical Bonding*; Oxford University Press: New York, 1997.

(3) Spackman, M. A. *J. Phys. Chem*. **1987**, *91*, 3179−3186. Spackman, M. A.; Weber, H. P.; Craven, B. M. *J. Am. Chem. Soc*. **1988**, *110*, 775−782.

(4) Boyd, R. J.; Choi, S. C. *Chem. Phys. Lett*. **1985**, *120*, 80−85. Boyd, R. J.; Choi, S. C. *Chem. Phys. Lett*. **1986**, *129*, 62−65.

(5) Carroll, M. T.; Chang, C.; Bader, R. F. W. *Mol. Phys*. **1988**, *63*, 387−405. Carroll, M. T.; Bader, R. F. W. *Mol. Phys*. **1988**, *65*, 695−722.

(6) Koch, U.; Popelier, P. L. A. *J. Phys. Chem*. **1995**, *99*, 9747−9754.

(7) Espinosa, E.; Molins, E.; Lecomte, C. *Chem. Phys. Lett*. **1998**, *285*, 170−173.

(8) Abramov, Yu. A. *Acta Crystallogr*. **1997**, *A53*, 264−272.

10.1021/ja983320f CCC: $18.00
Published on Web 03/09/1999

Table 1. Crystal Data and Structure Refinements for DL-Histidine

empirical formula	$C_6H_9N_3O_2$
fw	155.16
temp	110(2) K
wavelength	0.710 73 Å
cryst system	monoclinic
space group	$P2_1/c$
unit cell dimens	$a = 8.9886(1)$, $b = 7.945(1)$, $c = 9.3861(1)$ Å; $\alpha = \gamma = 90$, $\beta = 97.367(1)°$
V, Z	664.745(10) Å^3, 4
D(calcd)	1.550 Mg/m^3
abs coeff	0.119 mm^{-1}
F(000)	328 e
cryst size	0.10 × 0.10 × 0.10 mm
θ range	3.37−60.56°; $((\sin\theta)/\lambda)_{max} = 1.23$ Å^{-1}
limiting indices	$-20 \le h \le 21$, $-17 \le k \le 13$, $-19 \le l \le 22$
reflcns collcd	38 894
indpdt reflcns	9081 ($R_{int} = 0.0384$)
abs corr	none
refinement method	full-matrix least-squares on F^2
no. of params	136
goodness-of-fit on F^2	1.064 (spherical atom), 0.75 (aspherical atom)
final R indices	
spherical atom refinement [$I > 2\sigma(I)$]	$R_1 = 0.0503$ w$R_2 = 0.1126$
aspherical atom refinement [$I > 2.5\sigma(I)$]	$R_1 = 0.0296$ w$R_2 = 0.0457$

Thus, two quite different approaches are available. The first, based on electrostatics, must be complemented with other terms but can provide a physically meaningful basis for the calculation of the major electrostatic component of molecular interactions. The second, topological approach has not yet been applied to larger molecules, which are often connected through several intermolecular bond paths.

The importance of C−H···O and other electrostatic interactions in proteins is evident from a recent analysis of structures from the Protein Data Bank.[9] The charge density in crystals of amino acids and small polypeptides, which gives pertinent information, has been the focus of a number of experimental studies.[10−14] In the current work, 110 K CCD data on DL-histidine are used to analyze the intermolecular interactions in an amino acid crystal. Future studies will exploit the new experimental capabilities in the analysis of a number of well-diffracting polypeptides. Since the use of CCD detectors is quite recent, the data on DL-histidine have been checked for systematic bias by comparison with an earlier less extensive scintillation-counter data set collected at the same temperature.

Experimental Section

A colorless prism-shaped crystal with approximate dimensions 0.10 × 0.10 × 0.10 mm was used for 110 K data collection on a standard Bruker SMART CCD diffractometer and generator, operating at 2000 W power. The detector was positioned at 2.964 cm from the crystal. A total of 5280 frames were collected with a scan width of 0.3° in ω and an exposure time of 60 s/frame. The frames were integrated with the SAINT software package using a narrow frame integration method. Analysis of the data showed negligible decay during data collection. Details on the data collection and the cell dimensions are given in Table 1.

As this data set was the first set of CCD data used in our charge density studies, a careful comparison with the CAD4 data collected at the same nominal temperature by Li[15] was made. A plot of the ratios of the reflections common to both sets, obtained after the two sets have been brought to a common scale, is given in the Supporting Information (Figure S1a). A third-order polynomial fit to the ratios shows the higher order coefficients to be negligible and the slope of the resulting line to be only 0.0002. Clearly, there is no evidence for any intensity-dependent bias in the CCD data set. On the other hand, a Wilson plot of the logarithm of the ratios vs $((\sin^2\theta)/\lambda)^2$ (Figure S1b) has a slope of −0.14 Å^2, with the CAD4 data having the higher temperature factor. It is possible that the data collection temperatures were not exactly equal or, alternatively, that truncation of the high-order profiles occurred in the scintillation counter data collection. Assuming the temperature factors to be proportional to temperature, the difference translates into a ΔT of about 15 K, which is quite plausible.

The structure was solved and refined in the spherical-atom approximation using with the Bruker SHELXTL (version 5.0) Software Package. Positional and thermal parameters are listed in Tables S1 and S2, respectively. Bond lengths and angles (Table S3) are in agreement with those of the previous room-temperature structure determination of Edington and Harding[16] and with the 110 K structure of Li.[15]

Aspherical Atom Refinements

In the Hansen−Coppens multipole formalism[17] the atomic densities are described in terms of the spherical core and valence densities, augmented with an expansion of atom-centered spherical harmonic functions:

$$\rho_{at}(\mathbf{r}) = P_c\rho_{core}(r) + P_v\kappa^3\rho_{valence}(\kappa r) + \sum_{l=0}^{l_{max}}\kappa'^3 R_l(\kappa' r)\sum_{m=0}^{l} P_{lm\pm} d_{lm\pm}(\theta,\phi) \quad (1)$$

The populations P_v and $P_{lm\pm}$ and radial expansion/contraction parameters κ and κ' are treated as *charge density variables* in the least-squares refinement with aspherical form factors corresponding to the atoms

(9) Derewenda, Z. S.; Lee, L.; Derewenda, U. *J. Mol. Biol.* **1995**, *252*, 248−262.

(10) Destro, R.; Bianchi, R.; Morosi, G. *J. Phys. Chem.* **1989**, *93*, 4447−4457. Destro, R.; Biancchi, R.; Gatti, C.; Merati, F. *Chem. Phys. Lett.* **1991**, *186*, 47−52.

(11) Flaig, R.; Koritsanszky, T.; Zobel, D.; Luger, P. *J. Am. Chem. Soc.* **1998**, *120*, 2227−2238.

(12) Koritsanszky, T.; Flaig, R.; Zobel, D.; Krane, H.-G.; Morgenroth, W.; Luger, P. *Science* **1998**, *279*, 356−358.

(13) Howard, S. T.; Hursthouse, M. B.; Lehmann, C. W.; Poyner, E. A. *Acta Crystallogr.* **1995**, *B51*, 328−337.

(14) Souhassou, M.; Lecomte, C.; Blessing, R. H.; Aubry, A.; Rohmer, M.-M.; Wiest, R.; Bénard, M.; Marraud, M. *Acta Crystallogr.* **1991**, *B47*, 253−266. Souhassou, M.; Lecomte, C.; Ghermani, N.-E.; Rohmer, M.-M.; Wiest, R.; Bénard, M.; Blessing, R. H. *J. Am. Chem. Soc.* **1992**, *114*, 2371−2382.

(15) Li, N. Ph.D. Thesis, State University of New York at Buffalo, Buffalo, NY, 1989.

(16) Edington, P.; Harding, M. M. *Acta Crystallogr.* **1974**, *B30*, 204−206.

(17) Hansen, N. K.; Coppens, P. *Acta Crystallogr.* **1978**, *A34*, 909−921.

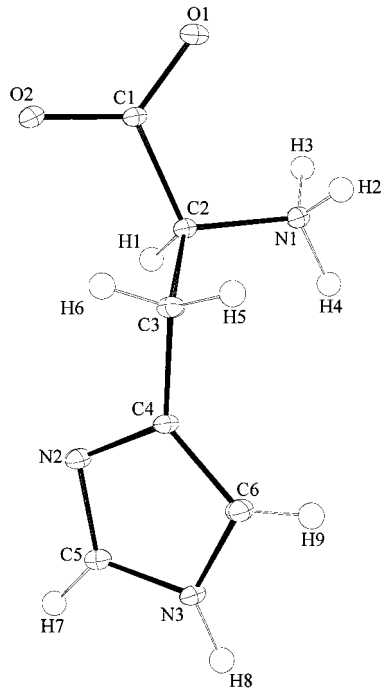

Figure 1. ORTEP drawing, showing 50% probability ellipsoids.

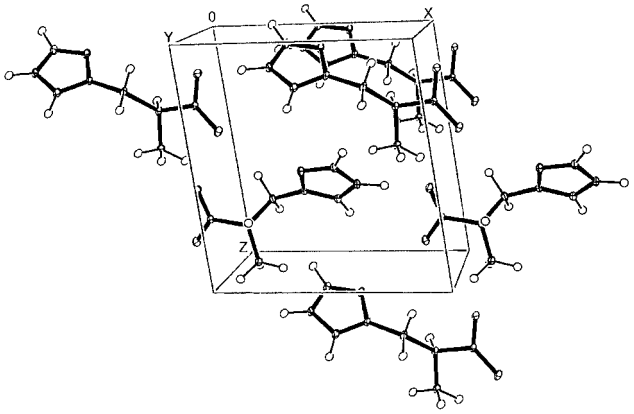

Figure 2. Packing diagram of the structure.

defined by (1). Such charge density variables are added to the positional and thermal parameters determined in a conventional structure analysis. The angular functions $d_{lm\pm}$ are real spherical harmonic functions and, thus, identical in shape to the atomic orbitals used in quantum chemistry. However, in charge density analysis they describe the density distribution rather than the wave function.

The refinements were carried out with the XD software package.[18] All non-hydrogen atoms were treated at the octupolar level, while an axially symmetric quadrupole was the highest pole on the H atoms. To reduce the number of charge density parameters, the atoms of the COO group, the β carbon atom, and the imidazole ring were assigned the local symmetry m and the NH_3 nitrogen atom was given C_{3v} symmetry. No symmetry restrictions were applied to the α carbon atom. All hydrogen atoms were treated as axially symmetric. Separate sets of population parameters were refined for C−H, N−H_3, and N−H hydrogen atoms. All κ values for the hydrogen atoms were fixed at 1.2. To eliminate instabilities in the refinement, it was necessary to constrain the κ parameters of the deformation functions (i.e. κ') of the two oxygen atoms to be equal.

The fit achieved in the aspherical atom refinement can be assessed by examination of the residual maps, calculated after completion of the refinement. The maps contain very little noise, attesting to the quality of the data; they do not show any features above 0.1 e Å^{-3} (Figure 3c). Final agreement factors of the aspherical atom refinement are included in Table 1. All structural results can be found in the Supporting Information. An ORTEP diagram with labeling of the atoms is shown in Figure 1 and a packing diagram is given in Figure 2, while model deformation densities in the plane of the carboxyl and imidazole groups are illustrated in Figure 3.

(18) Koritsanszky, T.; Howard, S. T.; Su, Z.; Mallinson, P. R.; Richter, T.; Hansen, N. K. *XD, Computer program package for multipole refinement and analysis of electron densities from diffraction data*; Free University of Berlin: Berlin, Germany, 1997.

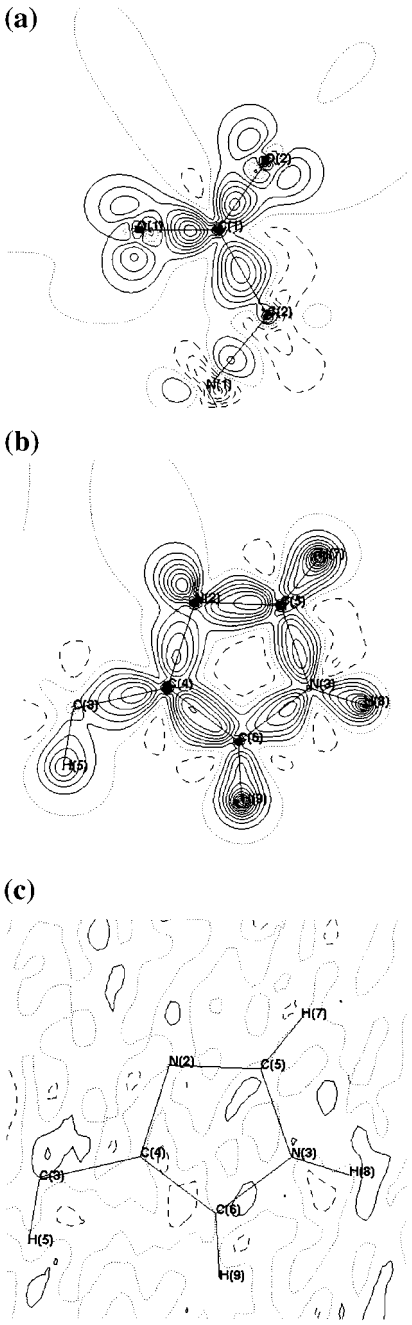

Figure 3. (a) Deformation density in the plane of the COO group, contours at 0.1 e Å^{-3} (zero contours dotted, negative contours broken). (b) Deformation density in the plane of the imidazole ring, contours as in (a). (c) Residual density in the plane of the imidazole ring, contours at 0.05 e Å^{-3}.

Theoretical Calculations

All theoretical calculations were performed with the Gaussian94 program package[19] using both Hartree−Fock and density functional methods. The largest basis set used was of 6-311++G(3df,3pd) quality. The molecular geometry as found in the crystal was adopted, to allow

Table 2. Total Energies of Histidine Molecule from the Theoretical Calculations

method		HF	B3LYP
basis set	6-311G**	6-311++G(3df,3pd)	6-311G**
no. of basis functions	252 (413 prim)	591 (752 prim)	252 (413 prim)
energy *E*, hartrees	−545.6012	−545.6650	−548.8655

comparison between theoretical and experimental results. Energies and molecular dipole moments from the monomer calculations are summarized in Table 2.

To compare experimental and theoretical molecular interaction energies, and the topology of the charge density in the intermolecular regions, molecular dimers were calculated with the eight different geometries existing in the monoclinic crystal. Calculations were performed at the HF/6-311G** and B3LYP/6-311G** levels. In the corresponding monomer calculations the basis-set superposition error was taken into account by the introduction of extra basis functions at the atomic positions of the second histidine molecule.[20]

Molecular and Electronic Structure of the Histidine Molecule

Molecular Geometry. The geometrical results are in excellent agreement with those obtained earlier by Li[15] (Table S3). The geometry determined in the room-temperature study of Edington and Harding is generally confirmed, though small significant differences are revealed in the current study, in which standard deviations have been significantly reduced. For instance, the two CO bonds of the carboxyl group, which were 1.248(5) and 1.252(5) Å according to the earlier results, are found to be 1.2449(5) and 1.2653(5) Å, for C−O(1) and C−O(2), respectively, in the current study. The difference may be explained by O(2) being the receptor atom in two N−H···O hydrogen bonds, while only one such interaction is found for O(1).

Electrostatic Moments. The electrostatic moments of a molecule in the crystal are obtained in a straightforward way from the atom-centered multipoles, which are produced in the aspherical atom refinement of the experimental structure factors.[2] To obtain reliable moments, the positions of the hydrogen atoms require special attention. While the bias in the X-ray hydrogen positions is reduced by use of aspherical atom scattering factors in the multipole refinement, the positions are generally less accurate than desirable. If no neutron data at the same temperature are available, the proton positions can be obtained by extending the X−H distances to their standard values. In the current work, the following values were used: C−H, 1.087 Å; N(NH_3)−H, 1.035 Å; N(imidazole)−H, 1.053 Å. The center of the hydrogen electron density is as determined by the aspherical atom X-ray analysis.

The experimental molecular dipole moment components were transformed to the inertial coordinate system of the histidine molecule for comparison with the results of the theoretical calculations. There is reasonable agreement between the relative values of the experimental and theoretical components (Table 3), indicating that the direction of the moment is correctly predicted. However, as observed previously, the magnitude of the dipole moment is enhanced in the crystal. The effect is most pronounced in comparison with the DFT calculations, which give a smaller dipole moment as at least part of the electron correlation is accounted for by the method. The difference between the isolated molecule and the crystal is due to polarization of the charge density in the field exerted by neighboring molecules. As shown by Gao and others, similar changes occur for molecules dissolved in polar solvents.[21] Compared with the DFT results, the dipole moment in the crystal is larger by 2 D, or about 15%. We note that in a number of other crystals much larger increases have been observed.[22]

That a similar enhancement already occurs in the dimer is evident from the theoretical results on a dimer consisting of two *a*-axis translation-related molecules in the crystal (1 + *X*, *Y*, *Z*; Figure 4). The DFT dipole moment of 29.41 D for the dimer exceeds twice the 14.40 D dipole moment of the monomer (Table 3). The increase is smaller, but only one other molecule is involved, rather than the 13 neighboring molecules in the crystal.

Table 3. Comparison of the Experimental and Theoretical Molecular Dipole Moments and Their Components (D) in the Inertial Coordinate System of the Histidine Molecule

	X	*Y*	*Z*	total
experiment	12.35	10.77	−2.47	16.57
HF/6-311G**	11.27	10.84	−2.30	15.80
HF/6-311++G(3df,3pd)	11.21	10.69	−2.22	15.65
B3LYP/6-311G**	10.18	9.97	−2.04	14.40

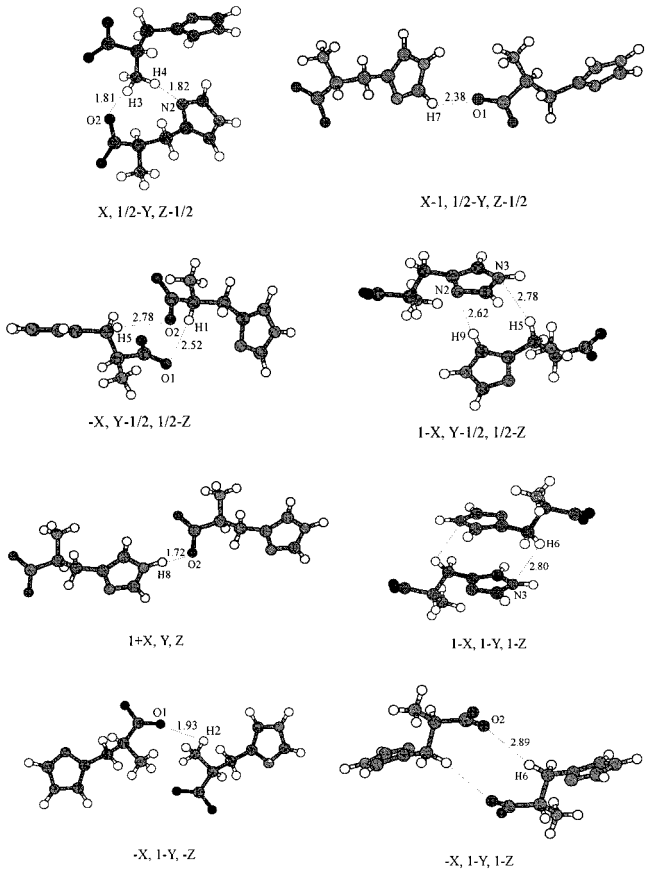

Figure 4. Geometry of the molecular pairs in the crystal.

(19) Frisch, M. J.; Trucks, G. W.; Schlegel, H. B.; Gill, P. M. W.; Johnson, B. G.; Robb, M. A.; Cheeseman, J. R.; Keith, T.; Petersson, G. A.; Montgomery, J. A.; Raghavachari, K.; Al-Laham, M. A.; Zakrzewski, V. G.; Ortiz, J. V.; Foresman, J. B.; Cioslowski, J.; Stefanov, B. B.; Nanayakkara, A.; Challacombe, M.; Peng, C. Y.; Ayala, P. Y.; Chen, W.; Wong, M. W.; Andres, J. L.; Replogle, E. S.; Gomperts, R.; Martin, R. L.; Fox, D. J.; Binkley, J. S.; Defrees, D. J.; Baker, J.; Stewart, J. P.; Head-Gordon, M.; Gonzalez, C.; Pople, J. A. *Gaussian 94, Revision E.2*; Gaussian, Inc.: Pittsburgh, PA, 1995.

(20) Boys, S. F.; Bernardi, F. *Mol. Phys.* **1970**, *19*, 553−566.

(21) Gao, J.; Xia, X. *Science* **1992**, *258*, 631−635. Gao, J. *Reviews in Computational Chemistry*; VCH: New York, 1996; Vol. 7. Gao, J.; Alhambra, C. *J. Am. Chem. Soc.* **1997**, *119*, 2962−2963.

(22) Howard, S. T.; Hursthouse, M. B.; Lehmann, C. W.; Mallinson, P. R.; Frampton, C. S. *J. Chem. Phys.* **1992**, *97*, 5616−5630.

Table 4. (3, −1) Critical Point Parameters of Histidine in DL-Histidine at 110 K

bond	ρ_B (e Å^{-3})	ϵ	λ_1 (e Å^{-5})	λ_2 (e Å^{-5})	λ_3 (e Å^{-5})	$\nabla^2\rho$ (e Å^{-5})
C1−O1 CCD	2.83(5)	0.12	−25.88	−23.08	11.16	−37.8(2)
C1−O1 theory[a]	2.59	0.075	−23.12	−21.50	35.82	−8.8
C1−O1 theory[b]	2.62	0.037	−25.11	−24.22	43.31	−6.0
C1−O1 theory[c]	2.73	0.081	−29.13	−26.94	41.54	−14.5
C1−O2	2.66(3)	0.08	−23.50	−21.86	11.19	−34.2(2)
	2.51	0.092	−21.64	−19.82	27.86	−13.6
	2.55	0.054	−23.62	−22.41	34.07	−12.0
	2.65	0.095	−27.12	−24.76	32.29	−19.6
C1−C2	1.73(1)	0.21	−12.05	−9.97	8.78	−13.24(4)
	1.64	0.066	−11.65	−10.93	9.24	−13.4
	1.75	0.057	−12.83	−12.14	6.95	−18.0
	1.77	0.077	−13.55	−12.58	7.81	−18.3
C2−N1	1.61(1)	0.45	−10.30	−7.13	10.10	−7.33(3)
	1.55	0.078	−8.78	−8.14	7.17	−9.7
	1.52	0.128	−7.71	−6.84	14.29	−0.3
	1.57	0.077	−9.53	−8.85	11.99	−6.4
C2−C3	1.56(1)	0.16	−9.91	−8.57	9.24	−9.24(3)
	1.59	0.021	−10.57	−10.36	8.58	−12.4
	1.67	0.017	−11.29	−11.10	6.81	−15.6
	1.69	0.018	−11.64	−11.43	7.33	−15.7
C3−C4	1.75(2)	0.07	−11.71	−10.95	11.33	−11.33(6)
	1.74	0.053	−12.14	−11.53	8.50	−15.2
	1.82	0.051	−12.95	−12.32	6.61	−18.7
	1.85	0.051	−13.53	−12.88	7.18	−19.2
C4−N2	2.16(3)	0.08	−16.18	−14.93	16.61	−14.5(1)
	2.10	0.135	−15.52	−13.68	8.05	−21.2
	2.14	0.117	−15.88	−14.21	7.84	−22.3
	2.29	0.130	−17.56	−15.54	5.66	−26.8
C5−N2	2.50(3)	0.19	−20.86	−17.50	15.68	−22.7(1)
	2.40	0.257	−19.32	−15.36	8.97	−25.7
	2.44	0.275	−20.56	−16.12	10.31	−26.4
	2.51	0.283	−22.53	−17.56	7.99	−32.1
C5−N3	2.27(3)	0.26	−18.97	−15.11	12.69	−21.4(1)
	2.13	0.202	−15.84	−13.18	13.22	−15.8
	2.14	0.138	−16.53	−14.52	20.87	−10.2
	2.23	0.180	−19.40	−16.44	17.69	−18.2
C6−N3	2.12(3)	0.13	−16.06	−14.16	13.34	−16.9(1)
	2.00	0.194	−13.97	−11.70	10.71	−15.0
	2.00	0.163	−14.19	−12.20	18.09	−8.3
	2.07	0.192	−16.65	−13.96	15.36	−15.2
C4−C6	2.23(3)	0.33	−17.52	−13.21	11.95	−18.78(9)
	2.18	0.348	−16.78	−12.45	7.59	−21.6
	2.24	0.438	−17.67	−12.28	5.38	−24.6
	2.29	0.420	−18.89	−13.30	6.43	−25.8
N1−H2	2.11(2)	0.02	−30.02	−29.47	32.78	−26.7(1)
	2.19	0.002	−29.51	−29.44	20.60	−38.4
	2.23	0.003	−30.78	−30.70	17.39	−44.1
	2.29	0.007	−32.38	−32.17	15.58	−49.0
N1−H3	2.05(2)	0.02	−28.71	−28.13	32.12	−24.72(4)
	2.19	0.003	−29.70	−29.60	20.35	−39.0
	2.22	0.004	−31.04	−30.93	17.12	−44.9
	2.29	0.008	−32.69	−32.45	15.06	−50.1
N1−H4	2.00(2)	0.03	−27.45	−26.77	31.43	−22.80(4)
	2.20	0.002	−28.93	−28.88	20.96	−36.8
	2.24	0.002	−30.17	−30.12	17.79	−42.5
	2.30	0.002	−31.61	−31.56	16.31	−46.9
N3−H8	2.61(4)	0.07	−38.71	−36.07	38.56	−36.2(3)
	2.06	0.043	−26.43	−25.35	20.12	−31.7
	2.09	0.046	−27.41	−26.20	17.34	−36.3
	2.15	0.044	−28.98	−27.75	15.77	−41.0
C2−H1	1.77(2)	0.14	−14.02	−12.32	11.93	−14.42(5)
	1.94	0.043	−19.01	−18.22	13.24	−24.0
	1.99	0.049	−19.26	−18.36	11.19	−26.4
	2.03	0.046	−20.34	−19.44	11.38	−28.4
C3−H5	1.91(1)	0.05	−16.41	−15.70	15.78	−16.33(4)
	1.87	0.022	−17.19	−16.82	11.67	−22.3
	1.91	0.025	−17.09	−16.85	9.18	−24.6
	1.95	0.024	−18.23	−17.80	9.79	−26.2
C3−H6	1.97(1)	0.04	−16.90	−16.24	15.18	−17.96(4)
	1.91	0.012	−18.61	−18.39	13.50	−23.5
	1.96	0.012	−18.84	−18.61	11.63	−25.8
	2.01	0.011	−19.83	−19.61	11.55	−27.9
C5−H7	2.06(3)	0.13	−21.39	−18.86	17.93	−22.3(1)
	1.91	0.049	−18.86	−17.98	13.11	−23.7
	1.97	0.043	−19.37	−18.57	11.48	−26.5
	2.03	0.041	−20.76	−19.94	11.65	−29.1
C6−H9	2.02(4)	0.12	−20.69	−18.41	18.82	−20.3(1)
	1.87	0.052	−18.04	−17.14	12.54	−22.6
	1.92	0.056	−18.28	−17.31	10.71	−24.9
	1.97	0.052	−19.54	−18.57	10.88	−27.2

[a] B3LYP/6-311G**. [b] HF/6-311G**. [c] HF/ 6-311G++(3df, 3pd). All critical point calculations were performed using AIMPAC95 software package (Biegler-König, F. W.; Bader, R. F. W.; Tang, T.-H. *J. Comput. Chem.* **1982**, *13* (3), 317).

Table 5. Comparison of Topological Parameters for Three Types of Bonds in a Number of Amino Acids[a]

bond	compd	R (Å)	ρ_b (e Å^{-3})	ϵ	λ_1 (e Å^{-5})	λ_2 (e Å^{-5})	λ_3 (e Å^{-5})	$\nabla^2\rho_b$ (e Å^{-5})
C1−O2	D,L-histidine	1.265	2.66	0.08	−23.5	−21.9	11.2	−34.2
	D,L-aspartic acid	1.255	2.87	0.29	−28.8	−22.4	15.1	−36.1
	D,L-proline	1.268	2.83	0.16	−29.5	−25.3	14.3	−40.5
	L-dopa	1.260	2.64	0.25	−28.2	−22.6	12.1	−38.8
	L-alanine	1.267	2.86	0.13	−27.6	−24.4	22.5	−29.5
C2−N1	D,L-histidine	1.483	1.61	0.45	−10.3	−7.1	10.1	−7.3
	D,L-aspartic acid	1.491	1.69	0.09	−13.0	−11.9	12.0	−12.9
	D,L-proline	1.504	1.67	0.19	−13.6	−11.4	15.1	−9.8
	L-dopa	1.495	1.62	0.47	−12.7	−8.6	12.9	−8.4
	L-alanine	1.488	1.70	0.30	−13.9	−10.7	13.6	−11.0
C1−C2	D,L-histidine	1.539	1.73	0.21	−12.1	−10.0	8.8	−13.2
	D,L-aspartic acid	1.537	1.69	0.25	−13.7	−10.9	11.7	−12.9
	D,L-proline	1.529	1.88	0.20	−15.4	−12.8	13.0	−15.2
	L-dopa	1.536	1.71	0.14	−12.5	−11.0	11.4	−12.0
	L-alanine	1.535	1.76	0.21	−13.5	−11.2	13.8	−10.9

[a] R, bond length; ρ_b, density at the bond critical point; ϵ, ellipticity of the bond; $\nabla^2\rho_b$, the Laplacian at the bond critical point; λ_1, λ_2, λ_3, principal components of $\nabla^2\rho_b$. References to data: DL-histidine, this work; DL-aspartic acid;[11] DL-proline;[12] L-dopa;[13] L-alanine.[10]

Topological Analysis of the Molecular Charge Density. In the theory of atoms in molecules[23] (AIM) the analysis of chemical bonding is firmly based on the topology of the total electron density. The theory is well-suited for the analysis of experimental charge densities. However, the electron density obtained by direct Fourier transform of the X-ray structure amplitudes cannot be used for this purpose because of experimental noise and incompleteness of the Fourier series. This is not the case for the analytical representation of the static density based on the parameters and functions of the multipole refinement.

The experimental topological parameters of the covalent bonds within the histidine molecule are listed in Table 4 and compared with both DFT and HF theoretical values. The largest discrepancies between theory and experiment occur for the λ_3 parameter, which represents the curvature along the bond path at the bond critical point. The disagreement is most pronounced for the polar C−O bonds and is much larger than the discrepancies between the various theoretical calculations. The *positions* of the critical points also disagree for these bonds, with the experimental critical points being closer to the carbon atoms. The same discrepancy was observed for L-alanine by Gatti et al.[24] and for DL-aspartic acid by Flaig et al.[11] These authors note that the agreement is improved when the comparison is made with the theoretical curvature at the experimental critical point position. As this position is not the critical point of the theoretical distribution, such a comparison seems less appropriate.

The agreement between theory and experiment is excellent for ρ_b, the density at the bond critical points, and very satisfactory for λ_1 and λ_2, the negative curvatures perpendicular to the bond path, which describe the contraction of the density into the bond. No clear trends are observed for the ellipticity ϵ, defined as $\lambda_1/\lambda_2 - 1$. Its value is quite dependent on small relative changes in λ_1 and λ_2.

Comparison of the topological properties of similar bonds in different amino acids (Table 5) shows the experimental results to be quite reproducible, with variations of a magnitude that may be expected, given the differences in chemical environment between molecules.

Analysis of the Intermolecular Interactions

Geometry of the Molecular Packing. Each molecule in the crystal is in contact with as many as 13 other neighboring molecules, with which it forms hydrogen-bond type interactions XH···Y with X= N, C and Y = O, N, C. The geometries of the molecular pairs in the crystal are shown in Figure 4, together with the symmetry relation between the two members of each of the pairs. Of the pairwise interactions, three involve a center of symmetry. In the five remaining cases, which involve a translational component, two identical interactions occur, where the central molecule is the acceptor of a hydrogen bond in one and the donor in the other case. Since all histidine molecules in the crystal are identical, this means that a molecule is the acceptor in one dimer and the donor in a second equivalent dimer. Thus, each histidine molecule has contacts with $3 + 2 \times 5 = 13$ neighboring molecules.

Electrostatic Contribution to the Molecular Interaction Energy. The electrostatic interaction energy between two nonoverlapping charge distributions can be calculated from the multipole moments of the distribution, as described by Buckingham.[25] The Buckingham expression is a series over interactions between multipoles of increasing order. Its convergence is much improved by use of the atom-centered multipoles rather than a single-site multipole expansion.

The electrostatic interaction energies based on the experimental atom-centered multipoles are listed in the first line of column four of Table 6. Examination of the contributions as a function of increasing order of the multipoles shows a reasonable convergence. The maximum contribution of the highest order octupole−octupole interaction is 1.9 kJ/mol and never exceeds 5.6% of the total electrostatic interaction energy.

To compare the results with commonly employed methods, a parallel calculation for the dimers in the histidine crystal was performed with the program CHARMM.[26] The electrostatic terms in the empirical CHARMM force field are based on monopoles only, with net charges determined by fitting ab initio interaction energies and geometries of complexes between water and a number of polypeptide model compounds. The charges for histidine in the CHARMM22 version of the potential[27] tend

(23) Bader, R. F. W. *Atoms in Molecules: A Quantum Theory*; Clarendon Press: Oxford, U.K., 1994.

(24) Gatti, C.; Bianchi, R.; Destro, R.; Merati, F. *J. Mol. Struct. (THEOCHEM)* **1992**, *255*, 409−433.

(25) Buckingham, A. D. In *Intermolecular Interactions from Diatomics to Biopolymers*; Pullman, B., Ed.; Wiley and Sons: Chichester, New York, 1978.

(26) Brooks, B. R.; Bruccoleri, R. E.; Olafson, B. D.; States, D. J.; Swaminathan, S.; Karplus, M. *J. Comput. Chem.* **1983**, *4*, 187−217.

(27) MacKerrell, A. D., Jr.; Bashford, D.; Bellot, M.; Dunbrack, R. L., Jr.; Evanseck, J. D.; Field, M. J.; Fischer, S.; Gao, J.; Guo, H.; Ha, S.; Joseph-McCarthy, D.; Kuchnir, L.; Kuczera, K.; Lau, F. T. K.; Mattos, C.; Michnick, S.; Ngo, T.; Nguyen, D. T.; Prodhom, B.; Reiher, W. E., III; Roux, B.; Schlenkrich, M.; Smith, J. C.; Stote, R.; Straub, J.; Watanabe, M.; Wiórkewicz-Kuczera, J.; Yin, D.; Karplus, M. *J. Phys. Chem. B* **1998**, *102*, 3586−3616.

Table 6. Energies of Intermolecular Interaction for Histidine Dimers

sym operation	bond path	$R_{H\cdots B}$ (Å)	E_{ES}[a] (kJ/mol)	$E_{ES} + E_{vdW}$[b] (kJ/mol)	E_{int}[c] (kJ/mol)	E_{int}[d] (kJ/mol)
$1 + X, Y, Z$	N−H(8)···O(2)	1.72	−97.8	−80.3	−70.6	−66.5
			−88.4	−86.0		
$X, {}^1/_2 - Y, Z - {}^1/_2$	N−H(3)···O(2)	1.81	−73.0	−80.6	−27.6	−32.7
	N−H(4)···N(2)	1.82	−81.0	−77.0		
	C(6)···H(7)−C	2.83				
$-X, 1 - Y, - Z$	N−H(2)···O(1)	1.93	−163.0	−155.5	−157.2	−153.7
	O(1)···H(2)−N		−203.6	−199.8		
$X - 1, {}^1/_2 - Y, Z - {}^1/_2$	O(1)···H(7)−C	2.38	+2.5	−1.4	−12.8	−13.6
			+3.6	+1.5		
$-X, Y - {}^1/_2, {}^1/_2 - Z$	C−H(1)···O(1)	2.52	−41.3	−54.6	−77.7	−66.6
	O(2)···H(5)−C	2.78	−104.2	−115.0		
$1 - X, Y - {}^1/_2, {}^1/_2 - Z$	N(2)···H(9)−C	2.62	−5.4	−18.4	+12.3	+6.6
	N(3)···H(5)−C	2.78	+8.4	−0.9		
$1 - X, 1 - Y, 1 - Z$	C−H(6)···N(3)	2.80	−32.1	−49.2	−5.9	−8.0
	N(3)···H(6)−C		−38.4	−52.2		
$-X, 1 - Y, 1 - Z$	C−H(6)···O(2)	2.89	+26.6	+20.1	+0.5	+1.5
	O(2)···H(6)−C		+21.8	+15.6		

[a] First line is multipole expansion of E_{es} for experimental charge density; second line is force-field calculations by CHARMM program. [b] E_{vdW} is exp-6 atom−atom potential as given by Cox et al.[28] and Williams and Cox;[29] O···H−X bonds, according to Mitchell and Price;[30] repulsion in other hydrogen bonds neglected. Second line is total intermolecular interaction energy calculated by CHARMM program. [c] HF/6-311G** calculation of the intermolecular interaction energy. [d] B3LYP/6-311G** calculation of the intermolecular interaction energy.

to be much larger than the experimentally determined charges, especially for the electronegative atoms. For instance, for the oxygen atoms of the carboxyl group the experiment gives −0.15 and −0.20 e for O(1) and O(2), respectively, while the charge used for the oxygen atoms of a terminal carboxyl group in CHARMM22 is −0.67 e. For the carbon atoms both the experimental and fitted charges are smaller and sometimes have the opposite sign. The differences are not surprising, as the CHARMM model is based on the monopoles only, so that the interaction between the higher poles must be absorbed into the monopole contribution.

The results of the CHARMM calculation for the dimers in the histidine crystal are listed on the second line of each cell in the column headed by E_{ES}. Given the different approximations involved, the qualitative agreement is rather striking. But a large discrepancy occurs for the pair of molecules related by the $-X$, $Y - {}^1/_2$, ${}^1/_2 - Z$ screw axis symmetry operation, for which CHARMM overestimates the interaction. A similar, but less pronounced, discrepancy occurs for the pair of molecules related by the inversion center at 0, ${}^1/_2$, 0 ($-X$, $1 - Y$, $-Z$). In both cases the point charge model gives a much larger stabilization than the multipole model.

In the column of Table 6 labeled $E_{ES} + E_{vdW}$, van der Waals interactions have been included. For the charge-density derived interactions this is done using the exp-6 atom−atom potential as parametrized by Cox and Williams,[28,29] complemented with the isotropic model of Mitchell and Price[30] for the O···H−X interaction. For the other hydrogen bonds, the repulsion term was omitted, as proposed by Spackman.[3] For the CHARMM results the standard parameters of the force field are used. The results show that the electrostatic interactions are dominant according to both methods, as noted for many other solids containing polar molecules.[31] The overall agreement is only slightly improved by the addition of the nonelectrostatic terms, which is perhaps not surprising, given the approximate nature of functions used to account for these contributions. In the molecular pair related by $-X$, $1 - Y$, $1 - Z$, listed at the end of Table 6, the interaction is repulsive, according to both the experimental and the CHARMM results, the two molecules being held together by the other cohesive forces in the crystal.

The results for the dimer calculations are listed in the last two columns of Table 6. The HF and DFT results agree reasonably well with each other, even though the HF calculations do not include the dispersive contribution and overestimate the electrostatic contribution since the charge separation is increased by the neglect of electron correlation (as is evident from the larger dipole moment). The supermolecule results are fairly close to those from the experimental charge-density analysis augmented with the van der Waals interactions, even though the comparison with theoretical results on an isolated dimer can only be semiquantitative. When discrepancies occur, the theoretical results tend to agree less well with the empirical force field predictions, as is evident especially for the $-X$, $1 - Y$, $-Z$ pair (the third pair listed in Table 6), for which the empirical and theoretical values are −199.8 and −153.7 kJ/mol (DFT), respectively.

Topology of Intermolecular Interactions. Earlier work has shown that, for all but the shortest hydrogen bonds, the electron density at the critical point ρ_{CP} is very low and the value of the Laplacian $\nabla^2\rho$ at the critical point is positive, a feature associated in the atoms in molecules (AIM) theory with closed-shell noncovalent interactions. As is evident from Table 7, this is also the case in the DL-histidine crystal. At first sight the agreement between the values of ρ_{CP} and $\nabla^2\rho$ according to experiment and those from HF/6-311G** and DFT calculations (listed in the second and third row of each entry in the table) is quite striking. But in fact the experimental and theoretical values are rather close to those of a superposition of promolecule densities (i.e. the superposition of spherical atoms), listed in the fourth line of each entry. Only for the three shortest hydrogen bonds in the table, NH(8)···O(2), NH(3)···O(2) and NH(4)···N(2), do the topological parameters reflect the effect of the intermolecular interaction. For these bonds the contraction into the bond path, described by the eigenvalues λ_1 and λ_2 of the Laplacian, is clearly more pronounced for the real crystal, and the value of λ_3 is higher.

The AIM theory relates the topological parameters of a bond with the energy of interaction. More specifically, for closed-shell interactions the functional of Abramov[8] expresses the

(28) Cox, S. R.; Hsu, L. Y.; Williams, D. E. *Acta Crystallogr*. **1981**, *A37*, 293−301.
(29) Williams, D. E.; Cox, S. R. *Acta Crystallogr*. **1984**, *B40*, 404−417.
(30) Mitchell, J. B. O.; Price, S. L. *Chem. Phys. Lett*. **1989**, *154*, 267−272.
(31) Coombes, D. S.; Price, S. L.; Willock, D. J.; Lesllie, M. *J. Phys. Chem*. **1996**, *100*, 7352−7360.

Table 7. Topological Properties of the Hydrogen Bonds in the Histidine Crystal[a]

Second molecule	hydrogen bond	R_{AB} (Å)	ρ_b (e/Å^3)	λ_1 (e/Å^5)	λ_2 (e/Å^5)	λ_3 (e/Å^5)	$\nabla^2\rho$ (e/Å^5)	G_{CP}[b] (au)	V_{CP}[c] (au)
$1 + X, Y, Z$	N−H(8)···O(2)	1.72	0.259(18)	−1.48	−1.44	5.67	2.75(3)	0.032	−0.035
			0.273	−1.65	−1.58	6.62	3.40	0.037	−0.039
			0.295	−1.78	−1.73	6.60	3.10	0.036	−0.039
			0.348	−1.83	−1.79	6.85	3.23		
$X, {}^1/_2 - Y, Z - {}^1/_2$	N−H(3)···O(2)	1.81	0.243(1)	−1.37	−1.32	5.17	2.47(1)	0.028	−0.031
			0.230	−1.26	−1.22	5.44	2.88	0.030	−0.030
			0.248	−1.35	−1.33	5.35	2.66	0.030	−0.030
			0.289	−1.42	−1.39	5.66	2.86		
	N−H(4)···N(2)	1.82	0.266(2)	−1.51	−1.44	5.49	2.54(2)	0.031	−0.035
			0.259	−1.44	−1.38	5.74	2.92	0.032	−0.034
			0.274	−1.51	−1.47	5.61	2.63	0.030	−0.034
			0.300	−1.40	−1.37	5.27	2.50		
	C(6)···H(7)−C	2.83	0.042(1)	−0.13	−0.09	0.76	0.55(1)	0.004	−0.003
			0.043	−0.13	−0.07	0.72	0.52	0.004	−0.003
			0.045	−0.13	−0.07	0.70	0.50	0.004	−0.003
			0.064	−0.16	−0.10	0.85	0.59		
$-X, 1 - Y, -Z$	N−H(2)···O(1)	1.93	0.165(5)	−0.79	−0.69	3.84	2.36(1)	0.022	−0.020
			0.174	−0.82	−0.76	4.07	2.49	0.023	−0.021
			0.188	−0.88	−0.83	4.01	2.30	0.022	−0.021
			0.223	−0.99	−0.95	4.34	2.39		
$X - 1, {}^1/_2 - Y, Z - {}^1/_2$	O(1)···H(7)−C	2.38	0.073(1)	−0.29	−0.27	1.55	0.98(1)	0.008	−0.006
			0.069	−0.25	−0.23	1.39	0.92	0.008	−0.007
			0.073	−0.25	−0.24	1.37	0.88	0.008	−0.006
			0.086	−0.29	−0.28	1.61	1.04		
$-X, Y - {}^1/_2, {}^1/_2 - Z$	C−H(1)···O(1)	2.52	0.054(2)	−0.18	−0.15	1.08	0.74(1)	0.006	−0.004
			0.053	−0.18	−0.17	0.97	0.62	0.006	−0.005
			0.055	−0.18	−0.17	0.93	0.59	0.005	−0.005
			0.067	−0.21	−0.17	1.18	0.69		
	O(2)···H(5)−C	2.78	0.032(1)	−0.10	−0.07	0.62	0.46(1)	0.004	−0.002
			0.037	−0.11	−0.10	0.63	0.43	0.004	−0.003
			0.038	−0.11	−0.09	0.60	0.40	0.004	−0.003
			0.046	−0.12	−0.05	0.69	0.53		
$1 - X, Y - {}^1/_2, {}^1/_2 - Z$	N(2)···H(9)−C	2.62	0.052(1)	−0.15	−0.08	0.89	0.67(1)	0.006	−0.004
			0.058	−0.18	−0.07	0.87	0.62	0.005	−0.005
			0.058	−0.18	−0.07	0.84	0.60	0.005	−0.004
			0.080	−0.21	−0.09	1.10	0.80		
	N(3)···H(5)−C	2.78	0.033(3)	−0.11	−0.07	0.67	0.50(1)	0.004	−0.003
			0.043	−0.13	−0.09	0.67	0.46	0.004	−0.004
			0.043	−0.13	−0.08	0.64	0.43	0.004	−0.003
			0.057	−0.16	−0.09	0.82	0.56		
$1 - X, 1 - Y, 1 - Z$	C−H(6)···N(3)	2.80	0.040(2)	−0.12	−0.09	0.81	0.60(1)	0.005	−0.003
			0.044	−0.12	−0.08	0.75	0.55	0.005	−0.004
			0.044	−0.12	−0.07	0.70	0.51	0.005	−0.004
			0.058	−0.14	−0.06	0.83	0.62		
$-X, 1 - Y, 1 - Z$	C−H(6)···O(2)	2.89	0.021(1)	−0.06	−0.02	0.42	0.33(1)	0.003	−0.002
			0.022	−0.07	−0.06	0.42	0.28	0.002	−0.002
			0.024	−0.07	−0.07	0.41	0.27	0.002	−0.002
			0.028	−0.08	−0.08	0.52	0.36		

[a] The first and the second lines are the results of the HF/6-311G** and B3LYP/6-311G** calculations of two histidine molecules at the crystal geometry; the third line is based on the experimental charge density; the fourth line on the independent atom model. [b] $G_{CP} = (3/10)(3\pi)^{2/3}(\rho_{CP})^{5/3} + \nabla^2\rho_{CP}/6$. [c] $V(\mathbf{r}) = {}^1/_4\nabla^2\rho(\mathbf{r}) - 2G(\mathbf{r})$.

kinetic energy density G at the bond critical point to the topological parameters:

$$G_{CP} = (3/10)(3\pi)^{2/3}\rho_{CP}{}^{5/3} + \nabla^2\rho_{CP}/6 \qquad (2)$$

The kinetic energy density $G(\mathbf{r})$ is in turn related to the potential energy density $V(\mathbf{r})$ through the local virial theorem, which in atomic units can be expressed as[23]

$$V(\mathbf{r}) = {}^1/_4\nabla^2\rho(\mathbf{r}) - 2G(\mathbf{r}) \qquad (3)$$

The resulting values for each of the intermolecular interactions are listed in the last two columns of Table 7. It is clearly of interest to relate the local density values at the bond critical point to the total energy of the bond. A simple empirical relationship between V_{CP} and the hydrogen bond energy E_{HB} has been derived by Espinosa et al.[7] from theoretical results on molecular dimers. In atomic units the relation is

$$E_{HB} = {}^1/_2V_{CP} \qquad (4a)$$

or

$$E_{HB}\ (\text{kJ/mol}) = 1313V_{CP}\ (\text{au}) \qquad (4b)$$

When applied to the individual interactions in histidine, this expression gives results that correlate poorly with the interaction energies of Table 6. The discrepancy is striking for the $(-X, 1 - Y, -Z)$ molecular pair, connected by an N−H···O hydrogen bond. Expression (4) with $V_{CP} = -0.020$ au gives −26 kJ/mol, while the total interaction energy between the two molecules according to Table 6 is at least −150 kJ/mol.

While this result is unsatisfactory, one should keep in mind that eq 4 was derived for theoretical calculations on molecular

dimers with mostly equilibrium geometries and that the interactions between two molecules are obtained from the topology of the bond paths. However, in a crystal the equilibrium is reached for the ensemble of all interactions, while individual hydrogen bonds may be strained by the other forces acting in the crystal. Taking into account this consideration, a more rigorous application of eq 4 would be the evaluation of the intermolecular interaction energy of a histidine molecule with all 13 neighboring molecules hydrogen-bonded to it in the crystal. When this is done, the values are −655.2 and −388.6 kJ/mol from the experiment and relation (4), respectively, compared with −505.8 kJ/mol from the supermolecule calculations. Though the discrepancies are still considerable, the qualitative agreement is now more reasonable, taking into account that the 14-molecule complex is in equilibrium only in the crystal and that the interaction energy evaluated additively neglects many-body effects. The evaluation of the relation between topology of the charge density and the intermolecular interaction energy requires further testing on additional systems.

Concluding Remarks

The experimental charge density is a logical starting point for the calculation of the electrostatic contribution to intermolecular interactions and the calibration of existing force fields. For a broader application of experimental charge densities to interactions in proteins, it will be necessary to test the methods used here with diffraction data on well-crystallizing polypeptides. Such studies are now underway using data collected at synchrotron sources.

Acknowledgment. Support of this work by the National Science Foundation (Grant CHE9615586) is gratefully acknowledged. We thank Dr. Jiali Gao of the Chemistry Department, SUNY at Buffalo, for consultations concerning the CHARMM force field.

Supporting Information Available: Tables of atomic parameters, bond lengths, and charge density parameters and a figure from the aspherical atom refinement (PDF). This material is available free of charge via the Internet at http://pubs.acs.org.

JA983320F